

# Recurrent Aligned Network for Generalized Pedestrian Trajectory Prediction

Yonghao Dong, Le Wang, Sanping Zhou, Gang Hua, and Changyin Sun

Institute of Artificial Intelligence and Robotics, Xi'an Jiaotong University

**Abstract.** Pedestrian trajectory prediction is a crucial component in computer vision and robotics, but remains challenging due to the domain shift problem. Previous studies have tried to tackle this problem by leveraging a portion of the trajectory data from the target domain to adapt the model. However, such domain adaptation methods are impractical in real-world scenarios, as it is infeasible to collect trajectory data from all potential target domains. In this paper, we study a task named generalized pedestrian trajectory prediction, with the aim of generalizing the model to unseen domains without accessing their trajectories. To tackle this task, we introduce a Recurrent Aligned Network (RAN) to minimize the domain gap through domain alignment. Specifically, we devise a recurrent alignment module to effectively align the trajectory feature spaces at both time-state and time-sequence levels by the recurrent alignment strategy. Furthermore, we introduce a pre-aligned representation module to combine social interactions with the recurrent alignment strategy, which aims to consider social interactions during the alignment process instead of just target trajectories. We extensively evaluate our method and compare it with state-of-the-art methods on three widely used benchmarks. The experimental results demonstrate the superior generalization capability of our method. Our work not only fills the gap in the generalization setting for practical pedestrian trajectory prediction but also sets strong baselines in this field.

**Keywords:** Pedestrian Trajectory Prediction, Domain Generalization

## 1 Introduction

Pedestrian trajectory prediction aims to estimate the future movements of pedestrians given their observed trajectories. This task is crucial in various applications such as autonomous driving [10, 15, 21], visual recognition [7, 16, 32], navigation [8, 12, 45], and video surveillance [6, 28, 46]. Despite significant progress in this field, pedestrian trajectory prediction remains challenging due to the domain shift problem. This problem arises when a model encounters scenes significantly different from its training dataset, resulting in performance degradation. For example, the motion styles of students on a university campus differ significantly from those of players on a basketball court. Consequently, a predictor trained on campus datasets (*e.g.*, SDD) may excel in that scene, but encounter difficulties with the basketball court datasets (*e.g.*, NBA), as depicted in Figure 1(a).

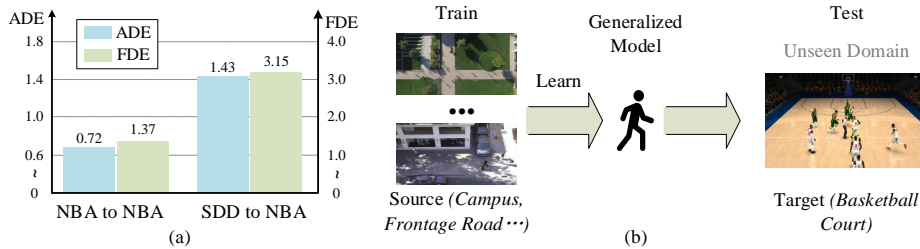


**Fig. 1:** (a) The graph shows performance decrease for SocialVAE [40], which demonstrates current work can’t address domain shift challenge well for pedestrian trajectory prediction. ‘A to B’ below X-axis denotes that the model is trained in source dataset ‘A’ and tested in target dataset ‘B’. (b) Definition of the generalized pedestrian trajectory prediction. In this generalization setting, the model is trained in multiple source domain datasets and tested in the target domain dataset.

Recent studies [11, 41] have identified the domain shift problem in pedestrian trajectory prediction and mitigate it through domain adaptation. However, in real-world scenarios like autonomous driving, domain changing is inevitable. Collecting trajectory data for all possible target domains is impractical, making the application of domain adaptation using data from target domains for model fine-tuning unfeasible in practice.

In this paper, we tackle the challenge of predicting pedestrian trajectories in an unseen target domain dataset, without requiring data from the target domain during model training, as illustrated in Figure 1(b). We term this task as Generalized Pedestrian Trajectory Prediction. One effective method to address this challenge is through domain alignment, which minimizes the data distribution gap between the source and target domains in high-dimensional feature spaces by using alignment losses such as Maximum Mean Discrepancy (MMD) [22], Correlation Alignment Distance (CORAL) [33], and adversarial loss [39]. Nevertheless, traditional domain alignment strategies are not well suited for pedestrian trajectory prediction tasks because 1) they align different domains directly, without considering the alignment at both time-state and time-sequence levels within trajectories; 2) they overlook the surrounding alignment, ignoring that the predicted trajectory is not only associated with that specific trajectory but also related to other interconnected trajectories within the scene.

To address these issues, we introduce a Recurrent Aligned Network (RAN), a new alignment framework tailored for generalized trajectory prediction, as illustrated in Figure 2. RAN deals with domain alignment by considering both time-state and time-sequence alignments, along with the social interaction dynamics inherent in pedestrian trajectories. This advancement is facilitated by two key modules: a recurrent alignment module and a pre-aligned representation module. The recurrent alignment module aims to minimize the domain gap at both time-state and time-sequence levels by a novel recurrent alignment strategy. Specifically, we first input trajectory representations from different domains at the starting timestamp into the GRU units and update the network using

alignment losses calculated by the output latent variables. Then, we input the trajectory representations of the next timestamp and the previously aligned latent variables into GRU and update the network with the new alignment losses. This iterative process continues until all timestamps’ trajectory representations have been processed, enabling the network to grasp generalized trajectory features across different domains, thereby aligning the gap between domains. Furthermore, the pre-aligned representation module focuses on accounting for the interactions among trajectories at each timestamp for more comprehensive alignment, achieved through stepwise attention mechanisms. Social interactions along with the target trajectory features are regarded as trajectory representations at each timestamp, which are used for the recurrent alignment.

Extensive experiments on three widely used benchmarks, including the ETH-UCY dataset [17, 27], SDD [29], and NBA dataset [43], show that our method outperforms all existing methods and demonstrate our superior generalization capabilities. The main contributions of our work are summarized as three-fold:

- We study a brand new setting, named generalized pedestrian trajectory prediction. We perform a rigorous study of existing state-of-the-art methods and establish strong baselines in the setting of domain generalization.
- We propose a Recurrent Aligned Neural Network to enhance the model’s generalization capability for generalized pedestrian trajectory prediction.
- We present a recurrent alignment module to minimize the domain gap at both time-state and time-sequence levels. Furthermore, we introduce a pre-aligned representation module, which considers social interactions instead of solely target trajectories, into the domain alignment process.

## 2 Related Works

### 2.1 Pedestrian Trajectory Prediction

The objective of pedestrian trajectory prediction [5, 25, 49] is to anticipate future movements of pedestrians based on the observed trajectories and their surrounding context. This task faces several challenges, including human interactions [2, 20, 31], multimodality [3, 30, 40], long-tail distribution [38], and momentary prediction [34]. To tackle human interaction, SGCN [31] introduces a sparse graph convolution network designed to model sparse directed interactions and motion tendencies. GP-Graph [2] considers both individual-specific and group-based relationships, representing them as graph structures. In terms of multimodality, SIT [30] proposes a social interpretable tree to represent various possible future trajectories. SocialVAE [40] employs a conditional variational autoencoder (CVAE) to capture the distribution of multimodal future trajectories within a latent space. To handle the long-tail distribution problem, FEND [38] introduces an improved contrastive learning framework to effectively identify less frequent trajectory patterns. For momentary prediction, MOE [34] incorporates a momentary observation feature extractor, allowing efficient use of valuable momentary information in the prediction process. The recent work, T-GNN [41],

has identified the domain shift problem and introduced a domain adaptation setting for pedestrian trajectory prediction. In this paper, we concentrate on a more practical setting, *i.e.*, domain generalization, to tackle the domain shift problem for pedestrian trajectory prediction.

## 2.2 Domain Generalization

Domain generalization (DG) [13, 19, 36, 44] aims to acquire representations that remain invariant across various domains, enabling the model to effectively generalize to unfamiliar domains. Both domain generalization and domain adaptation (DA) [14, 24, 37, 47] tackle the challenges posed by domain shift. However, the most significant difference between DA and DG is that DG does not require access to the target domain during training. In real-world scenarios, DG is more practical and challenging than DA, mainly because collecting data from all target domains can be arduous in real-world situations. A previous work on pedestrian trajectory prediction [41] addresses the domain shift problem within the domain adaptation setting, which may be impractical in real-world scenarios. In a recent work, Frenet [42] solves the domain shift problem from the perspective of domain generalization. Nevertheless, it is important to note that this work focuses primarily on vehicle trajectory prediction, limiting its direct applicability to pedestrian trajectory prediction due to distinctions in scenarios, experimental settings, and technology frameworks.

DG methods encompass various methods such as domain alignment [4, 18], meta-learning [9, 36], and data augmentation [35, 48]. Among these methods, domain alignment [4, 18] stands out as a widely used and effective strategy in DG, with the aim of minimizing the difference between the source domains to learn the domain-invariant representations. The rationale behind domain alignment is that features invariant to the source domain shift should also be robust to any unseen target domain shift. However, previous domain alignment methods are not tailored for sequence prediction tasks such as pedestrian trajectory prediction, as they do not consider the time sequence and human interaction properties. In this paper, we enhance the domain alignment method by incorporating a recurrent alignment strategy, tailoring it to be applicable for generalized pedestrian trajectory prediction.

## 3 Our Method

The overall framework of the RAN is illustrated in Figure 2. Due to the property of the domain alignment method, RAN needs two source domains in the training process for alignment. RAN consists of three main components: 1) a pre-aligned representation module that models trajectory representations from each source domain for alignment, 2) a recurrent alignment module that aligns each trajectory domain from both the time-state and time-sequence levels, and 3) a trajectory decoder module that decodes the generalized trajectory features into multimodal future predictions.

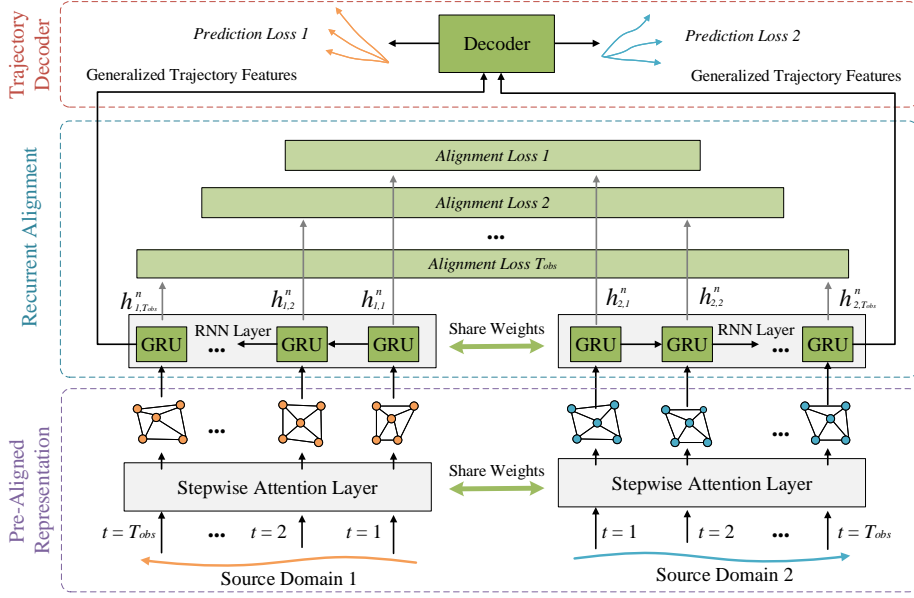


**Fig. 2:** The framework of the training phase of RAN. RAN need two source domains in the training process. Given trajectories of two different domains, we first model the pre-aligned representation of trajectories by the stepwise attention layers. Then we align the two domains' representation at both the time-state and time-sequence levels using the recurrent alignment module. Finally, we decode the well-aligned features (generalized trajectory features) into trajectory predictions. Note that the RNN layers and the stepwise attention layers share weights, respectively.

### 3.1 Problem Formulation

The objective of pedestrian trajectory prediction is to predict the future trajectory coordinates of the agent based on its observed trajectory and neighboring trajectories. Mathematically, given a pedestrian in domain  $i$ , let  $\mathbf{O}^i = [o_{i,1}, o_{i,2}, \dots, o_{i,T_{obs}}]$  be the observed trajectory over  $T_{obs}$  timestamps, where  $o_{i,t} \in \mathbb{R}^2$  denotes the 2D spatial coordinate at timestamp  $t$  in domain  $i$ . Let  $\mathcal{B}^i = [B_{i,1}, B_{i,2}, \dots, B_{i,T_{obs}}]$  be neighboring trajectories of  $\mathbf{O}^i$ , where  $\mathbf{B}_{i,t} \in \mathbb{R}^{2 \times a}$  is the 2D spatial coordinates of all neighboring trajectories at timestamp  $t$ .  $a$  is the number of neighbors. The future trajectory is  $\mathbf{Y}^i = [y_{i,T_{obs}+1}, y_{i,T_{obs}+2}, \dots, y_{i,T_{pred}}]$ , where  $y_{i,t} \in \mathbb{R}^2$  denotes the 2D spatial coordinate at timestamp  $t$  in domain  $i$ . The goal is to train a prediction model  $g(\cdot)$ , so that the prediction  $(\hat{\mathbf{Y}}^i)^{min}$  with minimum error in multimodal predictions  $(\hat{\mathbf{Y}}^i)^K = g(\mathbf{O}^i, \mathcal{B}^i)$  is as close to the ground truth  $\mathbf{Y}^i$  as possible.

Note that generalized pedestrian trajectory prediction requires training the model  $g(\cdot)$  in the source domains and testing  $g(\cdot)$  in different target domains. Due to the property of the domain alignment method, we incorporate two source domains during the training phase.

### 3.2 Pre-Aligned Representation

Pedestrian trajectory prediction is more challenging than traditional time-sequence prediction tasks, because it necessitates accounting for both the time-sequence property and the human interaction property at the time-state level. To capture the trajectory interactions within a scene at each timestamp, we adopt a step-wise attention mechanism to model the influence of neighboring trajectories on the agent to be predicted.

Given a trajectory  $\mathbf{O}^i$  in domain  $i$  and its neighboring trajectories  $\mathcal{B}^i$ , we first extract their high-dimensional feature embeddings at each timestamp as follows:

$$\mathbf{F}_{i,t}^o = f_o(o_{i,t}), \quad \mathbf{F}_{i,t}^b = f_b(B_{i,t}), \quad (1)$$

where  $\mathbf{F}_{i,t}^o$  and  $\mathbf{F}_{i,t}^b$  are the feature embeddings of  $o_{i,t}$  and  $B_{i,t}$ , respectively.  $f_o(\cdot)$  and  $f_b(\cdot)$  are nonlinear multilayer perceptron (MLP) encoders. To consider the influence of neighboring agents, we adopt the attention mechanism to model the social interaction at each timestamp as follows:

$$\begin{aligned} Q_{i,t} &= \phi(\mathbf{F}_{i,t}^o, W_{i,t}^q), \\ K_{i,t} &= \phi(\mathbf{F}_{i,t}^b, W_{i,t}^k), \\ V_{i,t} &= \phi(\mathbf{F}_{i,t}^b, W_{i,t}^v), \\ A_{i,t} &= \text{softmax}\left(\frac{Q_{i,t}(K_{i,t})^T}{\sqrt{d_k}}\right)V_{i,t}, \end{aligned} \quad (2)$$

where  $\phi(\cdot, \cdot)$  denotes the linear transformation.  $W_{i,t}^q$ ,  $W_{i,t}^k$  and  $W_{i,t}^v$  are learnable parameters.  $\mathbf{Q}_{i,t} \in \mathbb{R}^{1 \times d}$ ,  $\mathbf{K}_{i,t} \in \mathbb{R}^{a \times d}$ , and  $\mathbf{V}_{i,t} \in \mathbb{R}^{a \times d}$  are the query, key and value of the attention at timestamp  $t$  in domain  $i$ , respectively.  $\mathbf{A}_{i,t} \in \mathbb{R}^{1 \times d}$  is the output of the stepwise attention.  $\sqrt{d_k}$  is a scaled factor to ensure numerical stability. Hence, we can formulate the trajectory representation at timestamp  $t$  in domain  $i$  by considering the observation  $o_{i,t}$  and the stepwise attention  $A_{i,t}$  as follows:

$$X_{i,t} = \text{Concat}(Q_{i,t}, A_{i,t}), \quad (3)$$

where  $X_{i,t}$  is the time-state representation of the trajectory to be predicted at timestamp  $t$  in domain  $i$ .  $\text{Concat}(\cdot)$  denotes the concatenation operation.

Then, the representation of all trajectories in an arbitrary domain  $i$  can be constructed as follows:

$$\begin{aligned} F_i &= [\mathbf{f}_i^{(1)}, \mathbf{f}_i^{(2)}, \dots, \mathbf{f}_i^{(N_i)}], \\ \mathbf{f}_i^{(n)} &= [X_{i,1}^n, X_{i,2}^n, \dots, X_{i,T_{obs}}^n], n \in [1, \dots, N_i], \end{aligned} \quad (4)$$

where  $F_i$  is the feature space of all trajectories in domain  $i$ .  $N_i$  is the number of pedestrians in domain  $i$ .  $\mathbf{f}_i^{(n)}$  is the trajectory's pre-aligned representation of the  $n^{\text{th}}$  pedestrian over  $T_{obs}$  timestamps in domain  $i$ .  $X_{i,t}^n$  is the time-state representation of the  $n^{\text{th}}$  pedestrian's trajectory at timestamp  $t$  in domain  $i$ .

**Algorithm 1:** Recurrent Alignment Strategy

---

**Input:** Trajectory feature spaces of two source domains:  $F_1, F_2$ , where:  
 $F_i = [\mathbf{f}_i^{(1)}, \mathbf{f}_i^{(2)}, \dots, \mathbf{f}_i^{(N_i)}]$ ,  $\mathbf{f}_i^{(n)} = [X_{i,1}^n, \dots, X_{i,T_{obs}}^n]$ ,  $n \in [1, \dots, N_i]$ ,

- 1  $h_{i,t}^n \leftarrow X_{i,t}^n$  ▷ Equation 5
- 2  $S_{i,t} \leftarrow h_{i,t}^n$  ▷ Equation 6
- 3 **for**  $t = 1 : T_{obs}$  **do**
- 4   |  $\mathcal{L}_{rec}(t) \leftarrow [S_{1,t}, S_{2,t}]$  ▷ Equation 7
- 5 **end**
- 6  $\mathcal{L}_{rec} \leftarrow \sum_{t=1}^{T_{obs}} \mathcal{L}_{rec}(t)$  ▷ Equation 7
- 7 Backward Loss  $\mathcal{L}_{rec}$
- 8 Return

---

**3.3 Recurrent Alignment**

With the feature spaces  $[F_1, F_2]$  of two source domains not aligned properly, we aim to align them by minimizing the discrepancy of the two source domains. Then, we can assume that the resulting features will be domain-invariant and generalized well on the unseen target domains.

**Recurrent Alignment Strategy.** Different from traditional domain alignment strategies, the generalized pedestrian trajectory prediction task needs to consider the alignment at both the time-state and time-sequence levels. Prior to alignment, we first use a multilayer gated recurrent unit (GRU) RNN to model the high-dimensional features of the trajectory at both time-state and time-sequence levels for prediction in domain  $i$  based on hidden states. Each RNN layer calculates the recurrent information in the input trajectory sequence as follows:

$$\begin{aligned}
r_{i,t}^n &= \sigma(W_x^r X_{i,t}^n + W_h^r h_{i,t-1}^n + b^r), \\
z_{i,t}^n &= \sigma(W_x^z X_{i,t}^n + W_h^z h_{i,t-1}^n + b^z), \\
g_{i,t}^n &= \tanh(W_x^g X_{i,t}^n + r_{i,t}^n \odot W_h^g h_{i,t-1}^n + b^g), \\
h_{i,t}^n &= (1 - z_{i,t}^n) \odot g_{i,t}^n + z_{i,t}^n \odot h_{i,t-1}^n,
\end{aligned} \tag{5}$$

where  $h_{i,t}^n$  is the hidden state of the trajectory’s time-state representation  $X_{i,t}^n$ .  $r_{i,t}^n$ ,  $z_{i,t}^n$ , and  $g_{i,t}^n$  are the reset, update, and new gates, respectively.  $W$  and  $b$  denote learning parameters.  $\sigma$  is the activation function.  $\odot$  is the element-wise multiplication. The initial hidden state  $h_{i,0}$  is produced by a linear transformation of the feature embedding  $\mathbf{F}_{i,t}^b$ . Hence, the feature space of each domain at different timestamps can be represented as:

$$S_{i,t} = \sum_{n=1}^{N_i} h_{i,t}^n, \tag{6}$$

where  $S_{i,t}$  is the feature space of all trajectories in domain  $i$  at timestamp  $t$ . Given  $S_{i,t}$ , we can minimize the discrepancy between the two source domains using the proposed recurrent alignment strategy and the recurrent alignment losses

outlined in Algorithm 1. Then, our network is capable of modeling generalized trajectory features, which can be regarded as domain-invariant.

**Recurrent Alignment Loss.** The alignment loss is to minimize the discrepancy between source domains. To support the proposed recurrent alignment strategy, we design a recurrent alignment loss to minimize the discrepancy between the two source domains at both time-state and time-sequence levels as follows:

$$\mathcal{L}_{rec} = \sum_{t=1}^{T_{obs}} \|S_{1,t}, S_{2,t}\|_{\mathcal{H}}, \quad (7)$$

where  $\mathcal{L}_{rec}$  is the recurrent alignment loss, which calculates the total discrepancy between the two source domains at each timestamp through the recurrent alignment strategy.  $\|S_{1,t}, S_{2,t}\|_{\mathcal{H}}$  is the alignment loss at timestamp  $t$ , indicating the discrepancy measurement between two source domains. There are multiple choices for measuring such discrepancies, such as  $L_2$  distance, MMD, and CORAL. We explore six measurement functions in Section 4 and choose  $L_2$  distance loss in this work.

### 3.4 Prediction and Loss Function

Pedestrian trajectory prediction aims to predict future trajectories that closely match the ground truth. Through the pre-aligned representation module and the recurrent alignment module, we can obtain the generalized trajectory features. Then, we need to decode these features into predictions as follows:

$$(\hat{\mathbf{Y}}_i^n)^K = f_d(h_{i,T_{obs}}^n), \quad (8)$$

where  $(\hat{\mathbf{Y}}_i^n)^K$  is  $K$  predictions of the  $n^{th}$  pedestrian in domain  $i$  following previous best-of- $K$  metrics.  $f_d$  is a mixture of expert decoders, implemented by  $K$  MLP layers. We use the  $L_2$  distance loss as the prediction loss as follows:

$$\mathcal{L}_{pre} = \frac{1}{2 \times N_i} \sum_{i=1}^2 \sum_{n=1}^{N_i} \|\mathbf{Y}_i^n - (\hat{\mathbf{Y}}_i^n)^{min}\|_2, \quad (9)$$

where  $\mathcal{L}_{pre}$  is the prediction loss of all trajectories in all source domains.  $(\hat{\mathbf{Y}}_i^n)^{min}$  denotes the prediction with the minimum error in  $(\hat{\mathbf{Y}}_i^n)^k$ .

The overall network is trained end-to-end by minimizing the total loss function  $\mathcal{L}_{RAN}$  as follows:

$$\mathcal{L}_{RAN} = \lambda_1 \mathcal{L}_{rec} + \lambda_2 \mathcal{L}_{pre}, \quad (10)$$

where  $\lambda_1$  and  $\lambda_2$  are coefficients of the loss function.



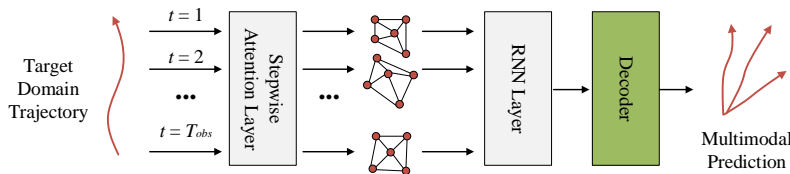


Fig. 3: The inference phase of the proposed RAN framework.

### 3.5 Inference

Because the two RNN layers share weights and the two stepwise attention layers share weights during training, the inference phase is straightforward, as illustrated in Figure 3. Given an observed trajectory from the target domain, we initially model its stepwise interaction using the stepwise attention layer. Subsequently, we combine this attention information with the trajectory embedding and input it into the well-aligned RNN layer to extract generalized trajectory features. Finally, we employ a multimodal trajectory decoder to decode the generalized trajectory features into the predicted trajectories.

## 4 Experiments and Discussions

### 4.1 Evaluation Datasets.

We evaluate our proposed method on three widely used benchmark datasets, each situated in different scenarios and representing different domains.

**ETH-UCY.** The ETH-UCY dataset [17,27] is captured in the scenes of outdoor pedestrian paths. It contains trajectories of 1,536 pedestrians in five subsets, *i.e.*, ETH, HOTEL, UNIV, ZARA1, and ZARA2. The trajectories within the ETH-UCY dataset are documented in world coordinates, and thus we report the results in meters as previous methods [1,40].

**SDD.** The Stanford Drone Dataset (SDD) [29] is captured in the scenes of university campus. It is a well established benchmark for human trajectory prediction in bird’s eye view, which consists of 20 subsets captured use a drone. Trajectories in SDD are documented in camera coordinates, and hence, we report the results in pixels as previous approaches [1,40].

**NBA.** The SportVU NBA movement (NBA) dataset [43] is captured in the scenes of basketball courts. It is a more challenging benchmark that contains rich social interactions. Due to the large size of the original dataset, we randomly extracted 257,230 trajectories in the “Rebound” subset following the previous method [40]. Trajectories in NBA dataset are documented in world coordinates, and hence, we report the results in meters as the previous approach [40].

### 4.2 Experimental Setting

**Evaluation Protocol.** We treat the three datasets, *i.e.*, ETH-UCY, SDD and NBA datasets, in different scenarios as different domains. For generalized pedes-

**Table 1:** Comparison for generalization results (ADE/FDE) on ETH-UCY. Model is trained on SDD and NBA. \* means the results are reproduced using the official released code. **Bold** indicates the best performance. The Lower the better.

Target Domain	Social-STG CNN* [26] CVPR2020	SGCN* [31] CVPR2021	TPNMS* [23] AAAI2021	GP-Graph* [2] ECCV2022	Social-VAE* [40] ECCV2022	Graph-TERN* [1] AAAI2023	<b>Ours</b>
ETH	0.66/0.92	0.72/1.16	0.69/0.97	0.54/0.76	0.57/0.79	0.53/0.74	<b>0.41/0.69</b>
UCY	0.68/0.99	0.52/0.79	0.63/0.90	0.27/0.63	0.45/0.66	0.25/0.58	<b>0.13/0.21</b>
UNIV	0.61/0.89	0.51/0.77	0.60/0.87	0.37/0.71	0.53/0.75	0.37/0.69	<b>0.25/0.46</b>
ZARA01	0.63/1.02	0.58/0.90	0.61/0.99	0.36/0.59	0.50/0.76	0.34/0.57	<b>0.22/0.41</b>
ZARA02	0.61/1.01	0.54/0.78	0.60/0.97	0.29/0.42	0.44/0.65	0.29/0.43	<b>0.16/0.31</b>
Average	0.64/0.97	0.57/0.88	0.63/0.94	0.37/0.62	0.49/0.72	0.36/0.60	<b>0.23/0.42</b>

trian trajectory prediction, the model can not reach the target domain data in the training phase. Specifically, taking source domains A and B and target domains C as examples, we split A, B and C into train sets and test sets, respectively. All train sets and the test set do not overlap. We train and validate the model on train and test sets of A and B, respectively. Then, we test the model on the test set of C. More details are given in the supplemental material.

**Evaluation Metrics.** Following previous methods [40, 41], we employ two commonly used metrics, *i.e.*, Average Displacement Error (ADE) and Final Displacement Error (FDE), as our evaluation metrics. ADE means the average  $L_2$  distance between all points of the prediction and ground truth. FDE means the  $L_2$  distance between the destination points of the prediction and ground truth.

**Implementation Details.** Similar with the previous methods [26, 40, 41], we calculate the best-of-20 performance. We observe 8 frames for each trajectory and predict the subsequent 12 frames. The two MLP encoders are all 2-layer linear transformations with the sigmoid activation function, and the hidden sizes are set to 64 and 128. The dimensions of the learnable parameters  $W_{i,t}^q$ ,  $W_{i,t}^k$ , and  $W_{i,t}^v$  in attention are all set to 256. We employ GRUs as the RNN structure. The activation function  $\sigma$  is sigmoid. The coefficients  $\lambda_1$  and  $\lambda_2$  in the loss function are set to 1. The Adam optimizer is used to train our model by 300 epochs with a learning rate of 0.001 and batch size of 512, decaying by 0.5 with an interval of 50, on one GTX-3090 GPU. We will release the code later for details.

### 4.3 Quantitative Analysis

Tables 1-3 show the performance compared to six state-of-the-art methods in three widely used datasets, which are regarded as three different domains. The model is trained on two selected domains and tested on the remaining one to evaluate cross-domain generalization. Consistent with established protocols, we express ETH-UCY and NBA results in meters and SDD results in pixels. To eliminate the impact of different units of measurement on the model, we unified them as meters during training. We reproduced previous state-of-the-art meth-

**Table 2:** Comparison for generalization results (ADE/FDE) on SDD. Model is trained on ETH-UCY and NBA. \* means the results are reproduced using the official released code. **Bold** indicates the best performance. The Lower the better.

Target Domain	Social-STG CNN* [26]	SGCN* [31]	TPNMS* [23]	GP-Graph* [2]	Social-VAE* [40]	Graph-TERN* [1]	<b>Ours</b>
SDD	23.24/36.49	20.44/32.53	25.43/38.56	16.79/27.02	17.12/28.06	14.76/25.47	<b>10.97/19.95</b>

**Table 3:** Comparison for generalization results (ADE/FDE) on NBA. Model is trained on ETH-UCY and SDD. \* means the results are reproduced using the official released code. **Bold** indicates the best performance. The Lower the better.

Target Domain	Social-STG CNN* [26]	SGCN* [31]	TPNMS* [23]	GP-Graph* [2]	Social-VAE* [40]	Graph-TERN* [1]	<b>Ours</b>
NBA	3.16/6.07	3.28/6.97	4.32/8.76	4.57/8.23	2.11/4.54	2.32/4.83	<b>1.28/2.64</b>

ods under the generalization setting through their official released codes without post-processing to ensure fair comparisons.

**ETH-UCY.** Table 1 shows the generalization performance on the ETH-UCY dataset. It shows that our method achieves the best performance in both ADE and FDE. Specifically, our method improves the average ADE/FDE from 0.36/0.60 to 0.23/0.42 compared to the previous best performance method, Graph-TERN [1]. Besides, we also outperform Graph-TERN in all five subsets, which demonstrates the superior generalization capability of our approach.

**SDD.** Table 2 shows the generalization performance on the SDD dataset. It shows that our method achieves the best performance in both ADE and FDE compared with the other methods. Specifically, our method improves the average ADE/FDE from 10.97/19.95 to 14.76/25.47 compared to the previous best performance method, Graph-TERN [1].

**NBA.** Table 3 shows the generalization performance on the NBA dataset. It shows that our method achieves the best performance in both ADE and FDE. Specifically, our method improves the average ADE/FDE from 1.28/2.64 to 2.11/4.45 compared to the previous best performance method, SocialVAE [40]. Notably, NBA dataset is captured in the basketball court, which presents denser interactions and a larger domain gap compared to the other datasets. Our method achieve more performance improvement facing such larger domain gap, *i.e.* 44.8%/45.3% (NBA), 36.1%/30% (ETH-UCY) and 25.6%/21.6% (SDD), compared with Graph-TERN [1]. These results underscore our method’s exceptional ability to generalize across varied and complex domains.

#### 4.4 Ablation Study

In this section, we first study the contribution of the important modules of RAN. Then we evaluate the impact of different alignment approaches. Finally, we study the impact of different alignment units and coefficients of our loss function.

**Table 4:** Ablation study of each components of our method in ADE/FDE in meters on ETH-UCY. The lower the better.

Variants	PAR	RA	ETH	HOTEL	UNIV	ZARA01	ZARA02	Average
(1)	✗	✗	0.50/0.81	0.21/0.40	0.31/0.58	0.29/0.57	0.20/0.38	0.30/0.55
(2)	✗	✓	0.43/0.73	0.16/0.29	0.30/0.57	0.27/0.54	0.19/0.37	0.27/0.50
(3)	✓	✗	0.46/0.77	0.18/0.33	0.26/0.47	0.23/0.45	0.18/0.32	0.26/0.47
(4)	✓	✓	<b>0.41/0.69</b>	<b>0.13/0.21</b>	<b>0.25/0.46</b>	<b>0.22/0.41</b>	<b>0.16/0.31</b>	<b>0.23/0.42</b>

**Table 5:** Ablation study of recurrent alignment loss on ETH-UCY dataset.

	MMD	CORAL	KLD	JS	COS	L2 (Ours)
ADE	0.32	0.30	0.25	0.27	0.32	<b>0.23</b>
FDE	0.58	0.55	0.45	0.49	0.56	<b>0.42</b>

**Contribution of Each Component.** We conduct two variants to evaluate the components of our RAN as shown in Table 4. PAR and RA denote the pre-aligned representation module and the recurrent alignment module, respectively. PAR is replaced by only embedding the target trajectory for recurrent alignment at each timestamp. RA is removed to evaluate our recurrent aligned strategy. The experimental results show that each component is effective in improving the generalization capability of our method.

**Analysis of Different Alignment Approaches.** As shown in Figure 4, we replace our recurrent alignment strategy in RAN with time-state and time-sequence alignment on the ETH-UCY dataset. “State” denotes time-state alignment, implemented by aligning the feature space at each step at attention layers. “Sequence” denotes time-sequence alignment, implemented by only aligning the feature space at the last step at RNN layers. “Recurrent” denotes our recurrent alignment strategy, which considers both time-state and time-sequence alignment. Experiment results show that our recurrent alignment strategy achieves the best performance, which indicates the superiority of our method in domain alignment for generalized pedestrian trajectory prediction.

**Analysis of Recurrent Alignment Loss.** As shown in Table 5, we conduct experiments to evaluate the impact of using different alignment losses as the alignment unit in  $\mathcal{L}_{rec}$ . Specifically, MMD, CORAL, KLD, JS, and COS denote using MMD loss, CORAL loss, Kullback-Leibler divergence loss, Jensen–Shannon divergence loss, and cosine similarity as the alignment unit in  $\mathcal{L}_{rec}$ , respectively. As mentioned in Section 3, we use the  $L_2$  distance as the alignment unit in  $\mathcal{L}_{rec}$ . The evaluation results suggest that the  $L_2$  distance is a more suitable domain distance measurement metric for pedestrian trajectory prediction tasks. One possible explanation is that high-dimensional feature representations may still preserve spatial-level information, *i.e.*, the spatial distance, in pedestrian trajectory prediction tasks.

**Analysis of Loss Coefficient.** As shown in Figure 5, we evaluate different loss coefficients to validate the appropriate proportion of the alignment module

in our framework. The proportion of the alignment module is represented by the figure’s loss coefficient ratio  $C = \lambda_1/\lambda_2$ . The evaluation results indicate that an excessive proportion of alignment modules sacrifices the model’s prediction accuracy, resulting in a performance decline. Conversely, a deficient proportion of alignment modules diminishes the model’s generalization capacity, leading to a performance decrease. Based on the experimental results, we choose  $C = 1$  in this work, which achieves the best performance.

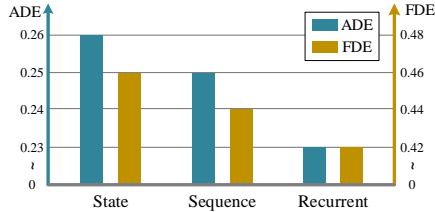


**Fig. 4:** Ablation study of different alignment approaches on ETH-UCY dataset. The lower the better.

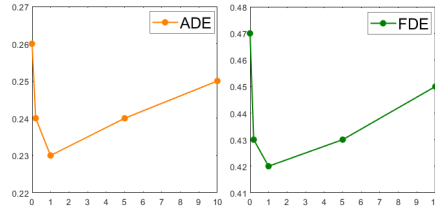


**Fig. 5:** Ablation study of using different loss coefficients on ETH-UCY dataset. X-axis is  $\lambda_1/\lambda_2$ . Y-axis is ADE or FDE.

## 5 Qualitative Analysis

**Feature Space Visualization.** As illustrated in Figure 6, we visualize the feature spaces under different domains using t-SNE. “w/ RA” and “w/o RA” denote with and without the RA module, respectively. In each figure, we randomly select a test batch data for each domain. Each point in the figure represents the feature of one trajectory. Points in different colours denotes features in different domains. Among these three sets of figures, there is a notably higher feature overlap when using the RA module, demonstrating that our alignment strategy can learn generalized trajectory features. Notably, due to dense interaction, NBA has a more extensive domain gap with ETH-UCY and SDD. The results show that our approach makes feature alignment more obvious in the face of more significant domain gaps, such as ETH-UCY & NBA and SDD & NBA.

**Predicted trajectory Visualization.** As shown in Figure 7, We compare the visualized trajectories with the best performance methods, SocialVAE [40] and Graph-TERN [1], on ETH-UCY dataset. The model is trained on the source domains SDD and NBA. The results in five subsets show that our method surpasses the trajectory prediction accuracy of both SocialVAE and Graph-TERN. This enhanced accuracy is particularly evident in the finer details of the predicted trajectories. This enhancement in prediction accuracy after domain change can be attributed to the effective feature alignment employed in our approach.

## 6 Conclusion

In this paper, we propose and study a new task named generalized pedestrian trajectory prediction. This task aims to generalize the model to unseen domains

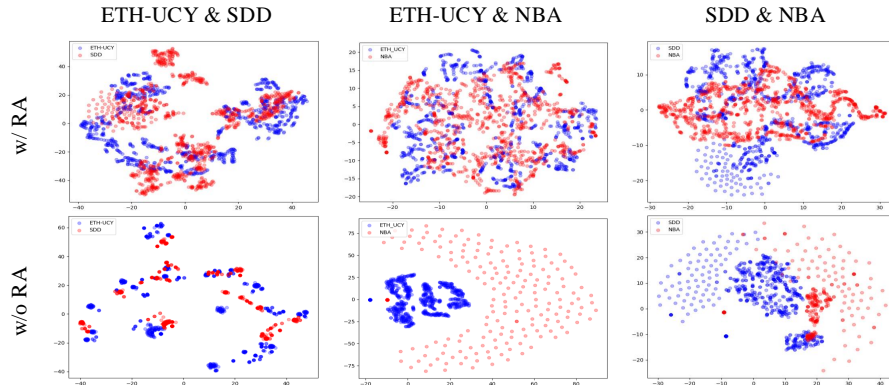


**Fig. 6:** Visualization of feature spaces of different domains using t-SNE. “A & B” on the top row denotes that the source domains are A and B during training. The blue and red dots denote feature spaces of corresponding source domain A and B, respectively. Deep colour regions indicate points overlap.

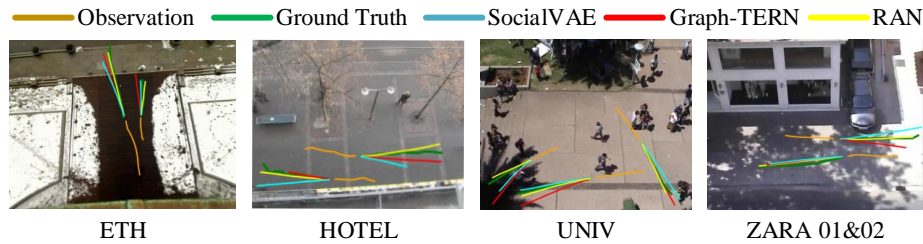


**Fig. 7:** Visualization of predicted trajectories compared with SocialVAE [40] and Graph-TERN [1] on ETH-UCY dataset.

without accessing the target domain trajectories in the training process. Furthermore, we propose the Recurrent Aligned Network (RAN), a novel alignment framework tailed for generalized pedestrian trajectory prediction. In RAN, we devise a recurrent alignment module with a recurrent alignment loss to effectively align different trajectory domains at both the time-state and time-sequence levels. In addition, we devise a pre-aligned representation module to consider human interactions during the domain alignment process. The experimental results unequivocally highlight the superior generalization capabilities of our method. To the best of our knowledge, our study is the first to explore the generalized setting for pedestrian trajectory prediction, offering significant insights for real-world autonomous driving systems.

**Limitation and Future Work.** One major limitation of our method is that we need two source domains in the training phase due to the characteristics of the domain alignment approach. In the future, we plan to tackle this problem by investigating a single-domain generalization solution for generalized pedestrian trajectory prediction.

## References

1. Bae, I., Jeon, H.G.: A set of control points conditioned pedestrian trajectory prediction. In: AAAI. vol. 37, pp. 6155–6165 (2023)
2. Bae, I., Park, J.H., Jeon, H.G.: Learning pedestrian group representations for multi-modal trajectory prediction. In: ECCV. pp. 270–289 (2022)
3. Bae, I., Park, J.H., Jeon, H.G.: Non-probability sampling network for stochastic human trajectory prediction. In: CVPR. pp. 6477–6487 (2022)
4. Chen, B., Liu, W., Yu, Z., Kautz, J., Shrivastava, A., Garg, A., Anandkumar, A.: Angular visual hardness. In: ICML. pp. 1637–1648 (2020)
5. Chen, G., Chen, Z., Fan, S., Zhang, K.: Unsupervised sampling promoting for stochastic human trajectory prediction. In: CVPR. pp. 17874–17884 (2023)
6. Chen, X., Peng, H., Wang, D., Lu, H., Hu, H.: Seqtrack: Sequence to sequence learning for visual object tracking. In: CVPR. pp. 14572–14581 (2023)
7. Du, F., Yang, P., Jia, Q., Nan, F., Chen, X., Yang, Y.: Global and local mixture consistency cumulative learning for long-tailed visual recognitions. In: CVPR. pp. 15814–15823 (2023)
8. Du, H., Li, L., Huang, Z., Yu, X.: Object-goal visual navigation via effective exploration of relations among historical navigation states. In: CVPR. pp. 2563–2573 (2023)
9. Du, Y., Xu, J., Xiong, H., Qiu, Q., Zhen, X., Snoek, C.G., Shao, L.: Learning to learn with variational information bottleneck for domain generalization. In: ECCV. pp. 200–216 (2020)
10. Hu, Y., Yang, J., Chen, L., Li, K., Sima, C., Zhu, X., Chai, S., Du, S., Lin, T., Wang, W., Lu, L., Jia, X., Liu, Q., Dai, J., Qiao, Y., Li, H.: Planning-oriented autonomous driving. In: CVPR. pp. 17853–17862 (2023)
11. Ivanovic, B., Harrison, J., Pavone, M.: Expanding the deployment envelope of behavior prediction via adaptive meta-learning. In: ICRA. pp. 7786–7793 (2023)
12. Kamath, A., Anderson, P., Wang, S., Koh, J.Y., Ku, A., Waters, A., Yang, Y., Baldrige, J., Parekh, Z.: A new path: Scaling vision-and-language navigation with synthetic instructions and imitation learning. In: CVPR. pp. 10813–10823 (2023)
13. Kang, J., Lee, S., Kim, N., Kwak, S.: Style neophile: Constantly seeking novel styles for domain generalization. In: CVPR. pp. 7130–7140 (2022)
14. Kennerley, M., Wang, J.G., Veeravalli, B., Tan, R.T.: 2pcnet: Two-phase consistency training for day-to-night unsupervised domain adaptive object detection. In: CVPR. pp. 11484–11493 (2023)
15. Khan, A.H., Nawaz, M.S., Dengel, A.: Localized semantic feature mixers for efficient pedestrian detection in autonomous driving. In: CVPR. pp. 5476–5485 (2023)
16. Lee, Y.L., Tsai, Y.H., Chiu, W.C., Lee, C.Y.: Multimodal prompting with missing modalities for visual recognition. In: CVPR. pp. 14943–14952 (2023)
17. Lerner, A., Chrysanthou, Y., Lischinski, D.: Crowds by example. *Comput. Graph. Forum* **26**(3), 655–664 (2007)
18. Li, H., Pan, S.J., Wang, S., Kot, A.C.: Domain generalization with adversarial feature learning. In: CVPR. pp. 5400–5409 (2018)
19. Li, L., Gao, K., Cao, J., Huang, Z., Weng, Y., Mi, X., Yu, Z., Li, X., Xia, B.: Progressive domain expansion network for single domain generalization. In: CVPR. pp. 224–233 (2021)
20. Li, L., Pagnucco, M., Song, Y.: Graph-based spatial transformer with memory replay for multi-future pedestrian trajectory prediction. In: CVPR. pp. 2231–2241 (2022)

21. Li, R., Shi, H., Fu, Z., Wang, Z., Lin, G.: Weakly supervised class-agnostic motion prediction for autonomous driving. In: CVPR. pp. 17599–17608 (2023)
22. Li, Y., Tian, X., Gong, M., Liu, Y., Liu, T., Zhang, K., Tao, D.: Deep domain generalization via conditional invariant adversarial networks. In: ECCV. pp. 624–639 (2018)
23. Liang, R., Li, Y., Li, X., Tang, Y., Zhou, J., Zou, W.: Temporal pyramid network for pedestrian trajectory prediction with multi-supervision. In: AAAI. vol. 35, pp. 2029–2037 (2021)
24. Liu, Y., Zhou, Z., Sun, B.: Cot: Unsupervised domain adaptation with clustering and optimal transport. In: CVPR. pp. 19998–20007 (2023)
25. Mao, W., Xu, C., Zhu, Q., Chen, S., Wang, Y.: Leapfrog diffusion model for stochastic trajectory prediction. In: CVPR. pp. 5517–5526 (2023)
26. Mohamed, A., Qian, K., Elhoseiny, M., Claudel, C.: Social-STGCNN: A social spatio-temporal graph convolutional neural network for human trajectory prediction. In: CVPR. pp. 14424–14432 (2020)
27. Pellegrini, S., Ess, A., Schindler, K., Van Gool, L.: You’ll never walk alone: Modeling social behavior for multi-target tracking. In: ICCV. pp. 261–268 (2009)
28. Rajasegaran, J., Pavlakos, G., Kanazawa, A., Feichtenhofer, C., Malik, J.: On the benefits of 3d pose and tracking for human action recognition. In: CVPR. pp. 640–649 (2023)
29. Robicquet, A., Sadeghian, A., Alahi, A., Savarese, S.: Learning Social Etiquette: Human trajectory understanding in crowded scenes. In: ECCV. pp. 549–565 (2016)
30. Shi, L., Wang, L., Long, C., Zhou, S., Zheng, F., Zheng, N., Hua, G.: Social interpretable tree for pedestrian trajectory prediction. In: AAAI. vol. 36, pp. 2235–2243 (2022)
31. Shi, L., Wang, L., Long, C., Zhou, S., Zhou, M., Niu, Z., Hua, G.: SGCN: Sparse graph convolution network for pedestrian trajectory prediction. In: CVPR. pp. 8990–8999 (2021)
32. Shu, Y., van den Hengel, A., Liu, L.: Learning common rationale to improve self-supervised representation for fine-grained visual recognition problems. In: CVPR. pp. 11392–11401 (2023)
33. Sun, B., Saenko, K.: Deep coral: Correlation alignment for deep domain adaptation. In: ECCV. pp. 443–450 (2016)
34. Sun, J., Li, Y., Chai, L., Fang, H.S., Li, Y.L., Lu, C.: Human trajectory prediction with momentary observation. In: CVPR. pp. 6467–6476 (2022)
35. Volpi, R., Namkoong, H., Sener, O., Duchi, J.C., Murino, V., Savarese, S.: Generalizing to unseen domains via adversarial data augmentation. *Advances in neural information processing systems* **31** (2018)
36. Wan, C., Shen, X., Zhang, Y., Yin, Z., Tian, X., Gao, F., Huang, J., Hua, X.S.: Meta convolutional neural networks for single domain generalization. In: CVPR. pp. 4682–4691 (2022)
37. Wang, W., Zhong, Z., Wang, W., Chen, X., Ling, C., Wang, B., Sebe, N.: Dynamically instance-guided adaptation: A backward-free approach for test-time domain adaptive semantic segmentation. In: CVPR. pp. 24090–24099 (2023)
38. Wang, Y., Zhang, P., Bai, L., Xue, J.: Fend: A future enhanced distribution-aware contrastive learning framework for long-tail trajectory prediction. In: CVPR. pp. 1400–1409 (2023)
39. Wu, Y., Inkpen, D., El-Roby, A.: Dual mixup regularized learning for adversarial domain adaptation. In: ECCV. pp. 540–555 (2020)
40. Xu, P., Hayet, J.B., Karamouzas, I.: Socialvae: Human trajectory prediction using timewise latents. In: ECCV. pp. 511–528 (2022)



41. Xu, Y., Wang, L., Wang, Y., Fu, Y.: Adaptive trajectory prediction via transferable gnn. In: CVPR. pp. 6520–6531 (2022)
42. Ye, L., Zhou, Z., Wang, J.: Improving the generalizability of trajectory prediction models with frenet-based domain normalization. arXiv preprint arXiv:2305.17965 (2023)
43. Yue, Y., Lucey, P., Carr, P., Bialkowski, A., Matthews, I.: Learning fine-grained spatial models for dynamic sports play prediction. In: 2014 IEEE international conference on data mining. pp. 670–679 (2014)
44. Zhang, H., Zhang, Y.F., Liu, W., Weller, A., Schölkopf, B., Xing, E.P.: Towards principled disentanglement for domain generalization. In: CVPR. pp. 8024–8034 (2022)
45. Zhang, S., Song, X., Li, W., Bai, Y., Yu, X., Jiang, S.: Layout-based causal inference for object navigation. In: CVPR. pp. 10792–10802 (2023)
46. Zhao, H., Wang, D., Lu, H.: Representation learning for visual object tracking by masked appearance transfer. In: CVPR. pp. 18696–18705 (2023)
47. Zhou, H., Chang, Y., Yan, W., Yan, L.: Unsupervised cumulative domain adaptation for foggy scene optical flow. In: CVPR. pp. 9569–9578 (2023)
48. Zhou, K., Yang, Y., Hospedales, T., Xiang, T.: Learning to generate novel domains for domain generalization. In: ECCV. pp. 561–578 (2020)
49. Zhu, D., Zhai, G., Di, Y., Manhardt, F., Berkemeyer, H., Tran, T., Navab, N., Tombari, F., Busam, B.: Ipc-tp: Utilizing incremental pearson correlation coefficient for joint multi-agent trajectory prediction. In: CVPR. pp. 5507–5516 (2023)